Supplementary Materials for

Error-prone chromosome-mediated spindle assembly favors chromosome segregation defects in human oocytes

Zuzana Holubcová, Martyn Blayney, Kay Elder, Melina Schuh*

*Corresponding author. E-mail: mschuh@mrc-lmb.cam.ac.uk

Published 5 June 2015, *Science* **348**, 1143 (2015)
DOI: 10.1126/science.aaa9529

This PDF file includes:

Other Supplementary Material for this manuscript includes the following:
(available at www.sciencemag.org/content/348/6239/1143/suppl/DC1)

Materials and Methods

Preparation and culture of human oocytes

The use of immature unfertilized human oocytes in this study has been approved by the UK's National Research Ethics Service under the REC reference 11/EE/0346. Immature unfertilized oocytes were donated by women receiving assisted reproduction treatment in Bourn Hall Clinic (Cambridge, UK) between September 2012 and December 2014. A total of 140 women aged 23–43 (mean patient age 33.5 ± 4.5) undergoing ovarian stimulation (*31*) for intracytoplasmic sperm injection (ICSI) took part in the study. Couples were referred to ICSI because of male factor associated infertility (70%), absence of a male partner (7.1%), polycystic ovary/anovulatory syndrome (5%), tubal damage (2.1%), endometriosis (1.4%), idiopathic infertility (12.8%) or a combination of these factors (1.4%). Only oocytes that were immature at the time of the ICSI procedure and thus could not be used for in vitro fertilization were used in this study. All patients participating in this study gave informed consent for these surplus oocytes to be used in this study. Live immature oocytes were collected within 5 hours after retrieval from ovaries and transported from Bourn Hall Clinic to the MRC LMB in a portable incubator (Hunter Scientific) at 37ºC in G-MOPS medium (Vitrolife) supplemented with 10% FBS (Fetal Bovine serum, 16000-044, Gibco). This allowed us to avoid freeze-thaw cycles which have been reported to have adverse effects on human oocytes (*32*). The oocytes were microinjected with 10-15 µl (1-2% of human oocyte volume) of 1-2 µg/µl mRNA encoding fluorescently labelled proteins using mercury-filled needles based on previously published methods (*9, 33*). To inhibit Ran, several oocytes from one patient were first microinjected with mRNAs encoding fluorescently labelled proteins and then split and microinjected with either 25 pl of His-RanT24N (2 mg/ml, RN05, Cytoskeleton) or corresponding amounts of BSA (Bovine serum albumin, A3311, Sigma). Oocyte culture, micromanipulation and live imaging were performed in G-MOPS medium supplemented with 10% FBS under mineral oil (Paraffin, Merck) at 37ºC. Only oocytes that were morphologically normal and underwent NEBD within 24 hours of retrieval from ovaries were used in this study.

Preparation and culture of mouse oocytes

All mice were maintained in a specific pathogen-free environment according to UK Home Office regulations. Oocytes were isolated from ovaries of 8-week-old FVBn mice, cultured and microinjected as described in detail before (*9*). Oocytes microinjected with mRNA encoding fluorescently labelled proteins were kept in medium supplemented with 250 µM dbcAMP (dibutyryl cyclic AMP) to maintain prophase arrest until the fluorescent proteins were expressed. Oocytes were then released into dbcAMP free medium. For immunofluorescence, mouse oocytes were isolated and cultured in dbcAMP free medium and fixed around 8 or 15 hours upon NEBD to obtain MI or MII spindles, respectively.

Confocal microscopy

Time-lapse image acquisitions were performed using a Zeiss LSM710 confocal microscope equipped with a Zeiss environmental incubator box with a 40x C-Apochromat 1.2 NA water immersion objective lens (Carl Zeiss). We typically recorded a volume of 130 µm x 130 µm x 70 µm (xyz), centered in z around the chromosomes. Image stacks were acquired every 10 minutes throughout oocyte maturation (from before NEBD until MII; ~24-48 hours). We either recorded only a single oocyte or multiple oocytes in parallel using Zeiss' MultiTime Series macro. EGFP was excited with a 488 nm argon laser line and emission detected within 492-543 nm. mRFP1 was excited with a 561 nm solid state laser and emission detected within 593-696 nm. Laser intensities were kept at a level that did not perturb oocyte development. Fixed cells were imaged on a Zeiss LSM710 or LSM780 confocal microscope with a 63x C-Apochromat 1.2 NA water immersion objective. In some images, shot noise was reduced with a Gaussian filter.

Expression constructs and mRNA synthesis

For in vitro mRNA synthesis, pGEMHE-H2B-mRFP1 (*9*) and pGEMHE-EGFP-MAP4 (*9*) were linearized with AscI. Capped mRNA was synthesized with T7 RNA polymerase (mMessage mMachine kit, Ambion) and dissolved in 11 µl water. mRNA concentrations were determined on ethidium bromide agarose gels by comparison with an RNA standard (Ambion).

Immunofluorescence

Oocytes, NHDF-Neo cells (normal human dermal fibroblasts – neonatal, CC-2509, Lonza; a gift from A. Hampl, Masaryk University, Brno, Czech Republic) and HEK 293 cells (human embryonic kidney 293 cells; gift from J. Howe, MRC LMB, Cambridge, UK) were fixed for 60 min at 37˚C in 100 mM HEPES (pH 7) (titrated with KOH), 50 mM EGTA (pH 7) (titrated with KOH), 10 mM MgSO4, 2% formaldehyde (MeOH free) and 0.2% Triton X-100, based on previously published methods (*34*). For cold treatments, oocytes were kept on ice for 6 min before they were fixed during early spindle assembly or ≥16 hours after NEBD to assess kinetochore-microtubule attachments close to anaphase onset. Oocytes were left in PBS, 0.1% Triton X-100 overnight at 4˚C. All antibody incubations were performed in PBS, 3% BSA and 0.1% Triton X-100, either overnight at 4ºC (for primary antibodies) or for 2 h at room temperature (for secondary antibodies). The primary antibodies used were rat anti-α-tubulin (MCA78G, Serotec; 1:3000), mouse anti-γ-tubulin (GTU88, Sigma; 1:500) and human ACA centromere CREST autoantibody *(*FZ90C-CS1058, Europa Bioproducts*;* 1:1000). Pericentrin in mouse oocytes was detected by a mouse anti-pericentrin antibody (611815, BD Biosciences; 1:750), and in human somatic cells and oocytes with a rabbit anti-pericentrin antibody (ab4448, Abcam; 1:1.500). As secondary antibodies, we used Alexa-Fluor-488 labelled anti-mouse, Alexa-Fluor-488 labelled anti-rat, Alexa-Fluor-488 labelled anti-rabbit, Alexa-Fluor-647 labelled anti-rat and Alexa-Fluor-647 labelled anti-human (all Molecular Probes; 1:400). DNA was stained with 0.5 µg/ml Hoechst 33342 (Molecular Probes).

General data analysis

To determine the stages of meiosis and to score for spindle instability, chromosome segregation and alignment defects, videos of live human oocytes were analyzed in 3D using the image analysis software Imaris (Bitplane). The timing of meiotic progression was quantified relative to the time of NEBD, which was defined as the time frame when the sharp boundary between the nucleus and the cytoplasm disappeared in the oocyte's differential interference contrast [DIC] image. Anaphase onset was defined as the time frame (10 minutes) before chromosome separation was first observed. Microtubule-kinetochore attachments in Fig. 4, A and B, fig. S4 and fig. S8 were determined by 3D analysis of high resolution deconvolved images (Huygens Professional) of the whole spindle volume. Kinetochore-microtubule attachments were only assessed in spindles that were oriented parallel to the imaging plane. Spindle poles were identified in 3D (Imaris) as regions of EGFP-MAP4 (in live cells) or α-tubulin (fixed cells) intensity that prominently protruded from the main microtubule mass. Oocytes whose spindles gradually increased in volume but maintained a detectable spindle axis and a barrel-shaped bipolar morphology were scored as having stable spindles. In the majority of oocytes, the spindle lost its initial bipolarity and its shape underwent dynamic remodeling. Oocytes with transient apolar spindles, in which the spindle had rounded up and a prominent spindle axis was absent, were scored as displaying moderate spindle instability. Oocytes, in which the spindle progressed through multipolar stages (frequently caused by widening and loosening of the spindle poles, followed by spindle pole splitting), were scored as displaying severe spindle instability.

Quantification of spindle volume

To quantify the spindle volume, the microtubule signal in oocytes expressing EGFP-MAP4 was segmented using the surface detection function in Imaris. A suitable threshold was selected at the time of anaphase onset and maintained for the entire series. The spindle volumes between NEBD and anaphase were then exported into Microsoft Excel for further processing. For Fig. 1D, data from individual oocytes were aligned to the time of NEBD and normalized to the spindle volume at the time of anaphase onset. For Fig. 1C and Fig. 2F, the data from individual oocytes were aligned to the time of NEBD, averaged and normalized to the average spindle volume for the whole data set (Fig. 1C) or average spindle volume of BSA injected control cells (Fig. 2F) at 16 hours after NEBD. The width and the length of MI and MII spindles (fig. S2, B and D) in live human oocytes expressing EGFP-MAP4 were measured in 3D in Imaris at anaphase onset (MI) and when a bipolar MII spindle had formed (MII).

Statistics

Average (mean), standard deviation (s.d.) and statistical significance based on Student's *t* test (two-tailed) for absolute values and Fisher's exact test (two-tailed) for category values were calculated in Microsoft Excel. All box plots show median (horizontal lines), mean (small squares), 25^{th} and 75^{th} percentiles (small boxes) and 5^{th}, 95^{th} percentiles (whiskers).

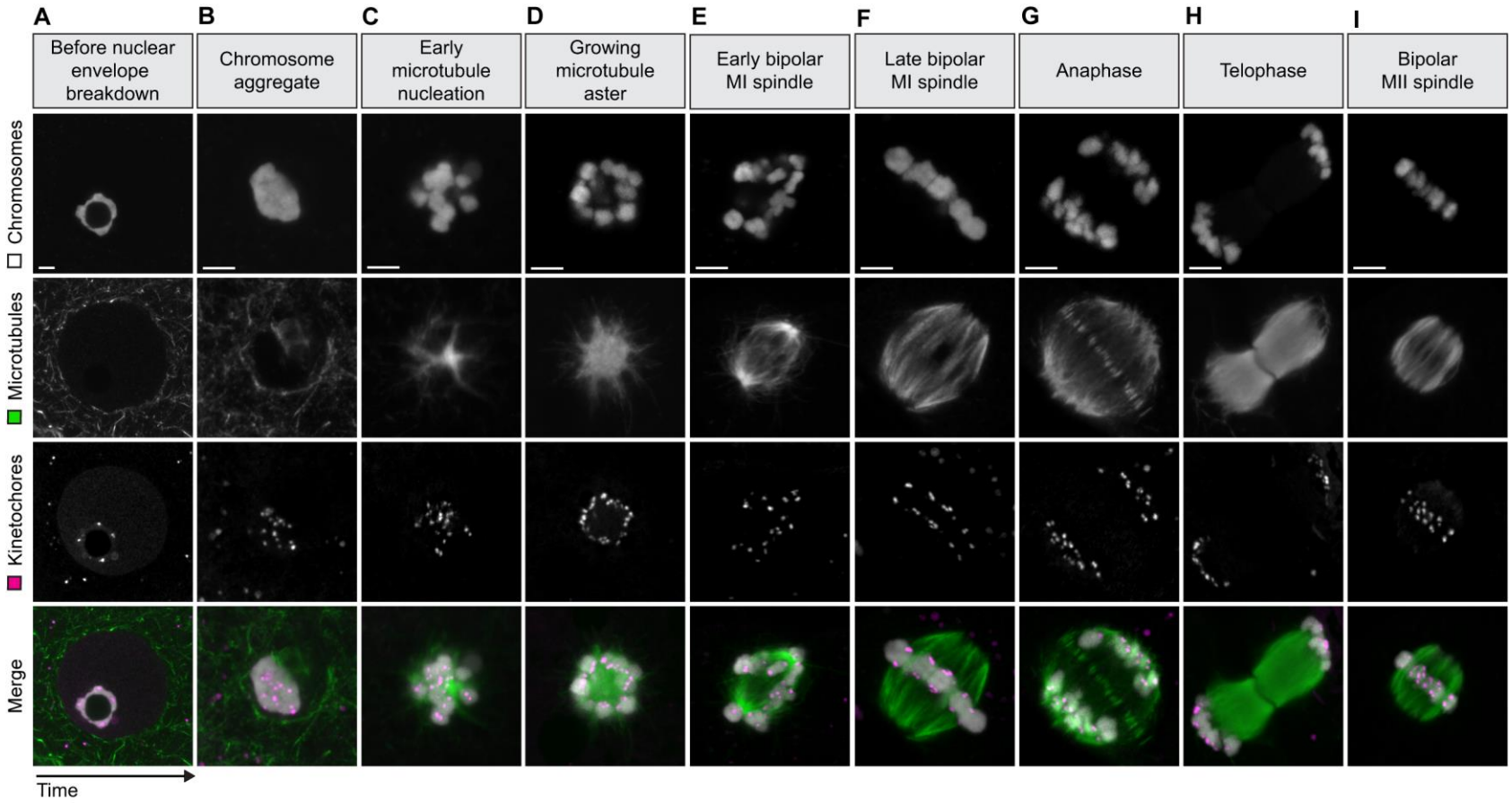

Fig. S1. Stages of meiosis in fixed human oocytes.

(**A to I**) The stages of meiosis observed in live oocytes were confirmed in oocytes that were not imaged but fixed at different time points before and after NEBD and immunostained for kinetochores (CREST) and microtubules (α-tubulin) together with chromosomes (Hoechst). *z* projections of six sections, every 0.3 μm. Scale bar, 10 μm.

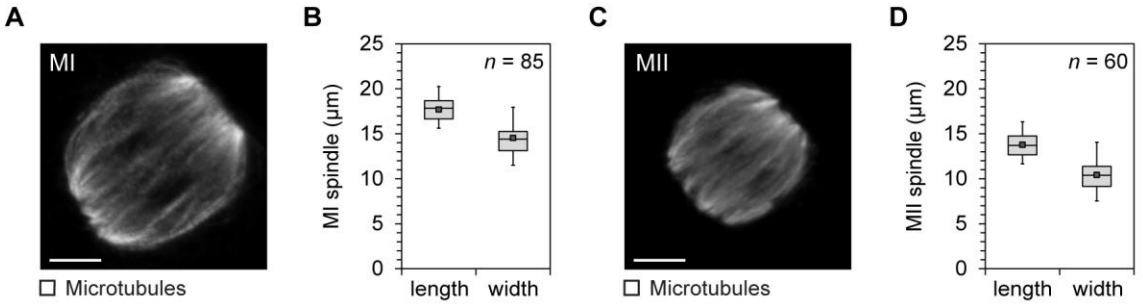

Fig. S2. Morphology of MI and MII spindles in human oocytes.

(**A** and **C**) Bipolar metaphase I (A) and metaphase II (C) spindles in fixed human oocytes are anastral, barrel-shaped and consist of loosely clustered bundles of microtubules. Immunofluorescence staining (*z* projection of six sections, every 0.3 µm) of microtubules (α-tubulin). Scale bar, 5 µm. See movie S2 for complete *z* stack.

(**B** and **D**) Length and width of metaphase I (B) and metaphase II (D) spindles were measured in 3D in live human oocytes expressing EGFP-MAP4 as shown in (Fig. 1A). Box plot is as in Fig. 1B. *n*, number of oocytes.

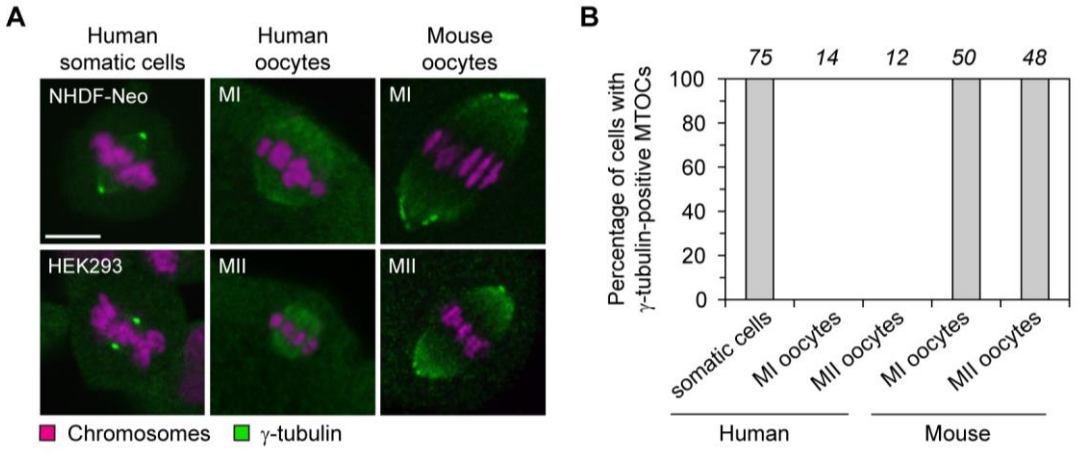

Fig. S3. Human oocytes lack detectable γ-tubulin-positive MTOCs

(**A**) Immunofluorescence staining of γ-tubulin together with chromosomes (Hoechst) in somatic cells (NHDF-Neo, normal human dermal fibroblasts-neonatal; HEK293, human embryonic kidney 293 cells), mouse and human MI and MII oocytes. γ-tubulin was detected on centrosomes in mitotic cells, and on MTOCs and minus ends of microtubules (diffuse staining in spindle area) in mouse oocytes. In human oocytes, γ-tubulin was detected on minus ends of microtubules (diffuse staining in spindle area), but not on distinct MTOCs. Scale bar, 10 µm.

(**B**) Spindles of somatic cells as well as metaphase I (MI) and metaphase II (MII) spindles in mouse and human oocytes as shown in (A) were scored for the presence of γ-tubulin-positive MTOCs. γ-tubulin-positive MTOCs could not be detected on human oocyte spindles. The number of cells is specified in italics.

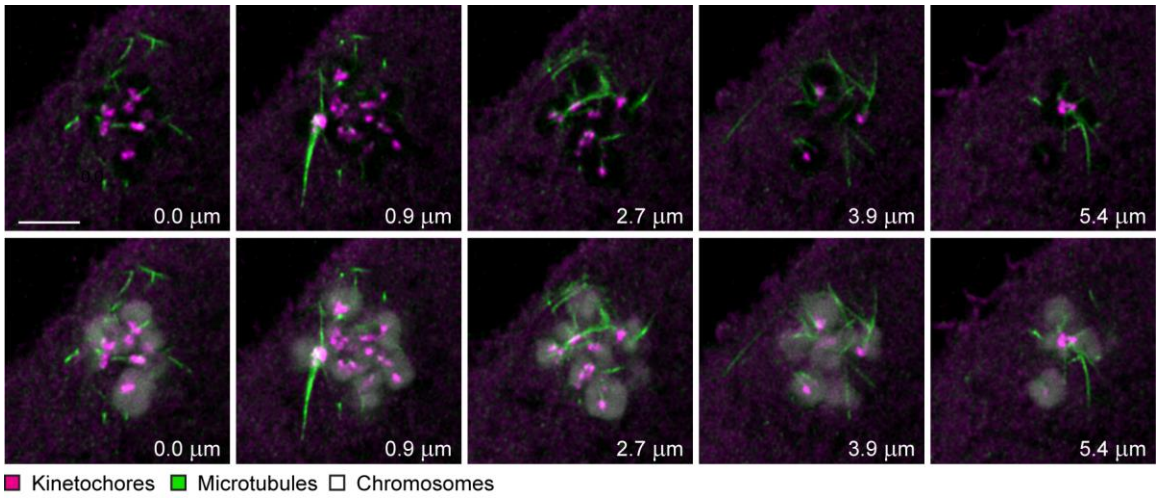

Fig. S4. Microtubules are initially nucleated on chromosomes.

High resolution images (figure shows individual sections of a *z* stack) of human oocytes fixed ~4 hours after NEBD show that microtubules (α-tubulin; green) are nucleated in the vicinity of chromosomes (Hoechst; white), emanating primarily from kinetochores (CREST; magenta). Images were deconvolved. Scale bar, 5 µm. See movie S3 for complete *z* stack.

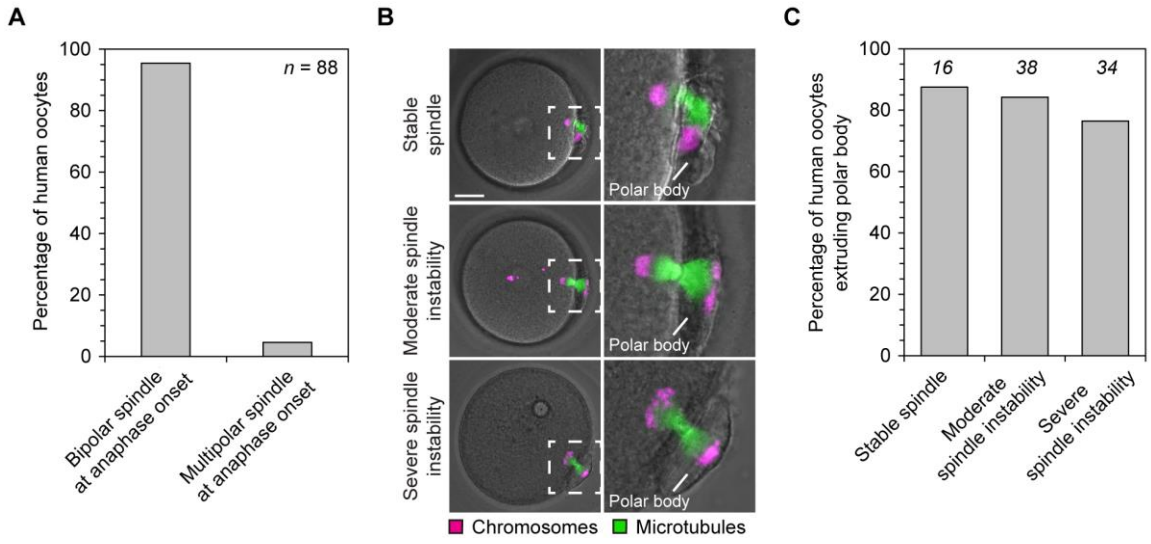

Fig. S5. Human oocytes recover from spindle instability before anaphase.

(**A**) Live human oocytes expressing H2B-mRFP1 (chromosomes) and EGFP-MAP4 (microtubules) as shown in (Fig. 1A) were scored for the presence of bipolar or multipolar spindles at anaphase onset. *n*, number of oocytes.

(**B**) Polar body extrusion in live oocytes with different degrees of spindle instability (same cells as in Fig. 3A). Oocytes expressing H2B-mRFP1 (chromosomes) and EGFP-MAP4 (microtubules) (*z* projections, four or six sections, every 4 or 5 µm merged with DIC) are shown. The outlined regions are magnified on the right. The magenta spheres in the cytoplasm of the cell with moderate spindle instability correspond to autofluorescent lipofuscin bodies frequently present in human oocytes (*35*). Scale bar, 25 µm.

(**C**) Rate of polar body extrusion was quantified in oocytes with different degrees of spindle instability. The number of oocytes is specified in italics.

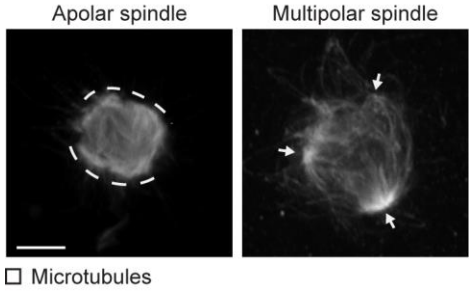

Fig. S6. Apolar and multipolar spindles in fixed human oocytes.

High resolution images (*z* projections of fifty sections, every 0.3 µm) of apolar and multipolar spindles in fixed human oocytes. Immunofluorescence of microtubules (α-tubulin). Arrows highlight defined spindle poles; dashed lines mark undefined spindle poles. Images indicate that spindle instability is also present in oocytes which have not been imaged. Scale bar, 5 µm.

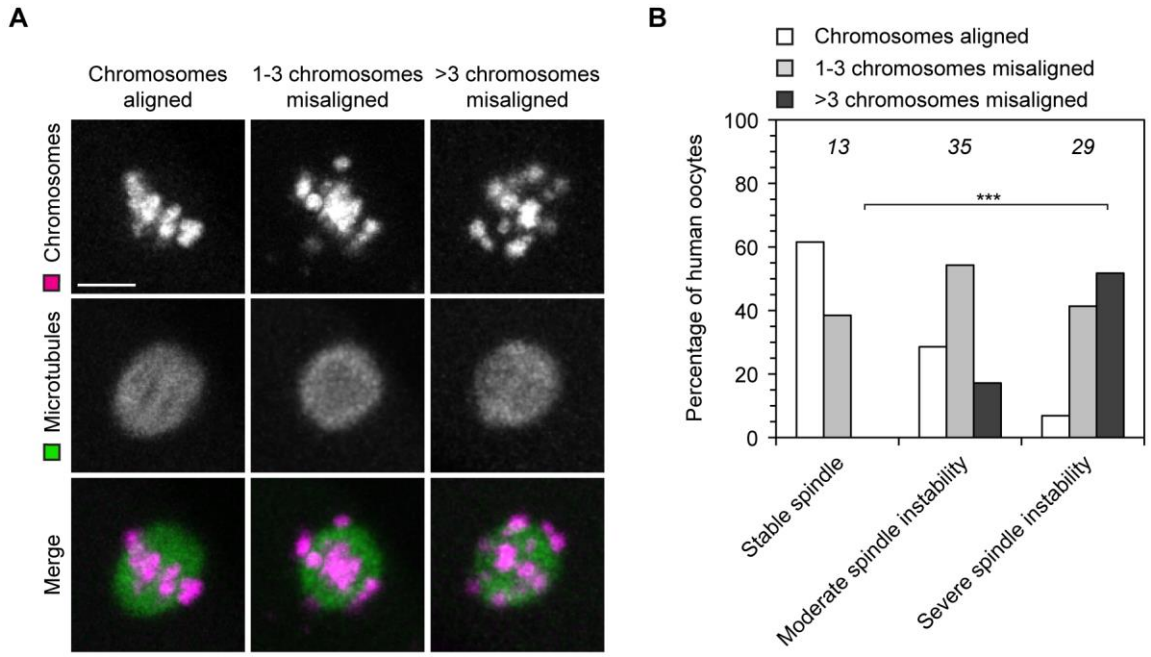

Fig. S7. Spindle instability correlates with chromosome alignment defects.

(**A**) Illustration of classes of chromosome alignment defects in live human oocytes expressing H2B-mRFP1 (chromosomes) and EGFP-MAP4 (microtubules). *z* projections of four sections, every 5 µm. Scale bar, 10 µm.

(**B**) Live human oocytes expressing H2B-mRFP1 (chromosomes) and EGFP-MAP4 (microtubules) as shown in (A) were scored for the presence of misaligned chromosomes at anaphase onset. Cells with unstable spindles are more likely to have misaligned chromosomes at anaphase onset. The number of oocytes is specified in italics. ***$P<10^{-4}$ (Fisher's exact test).

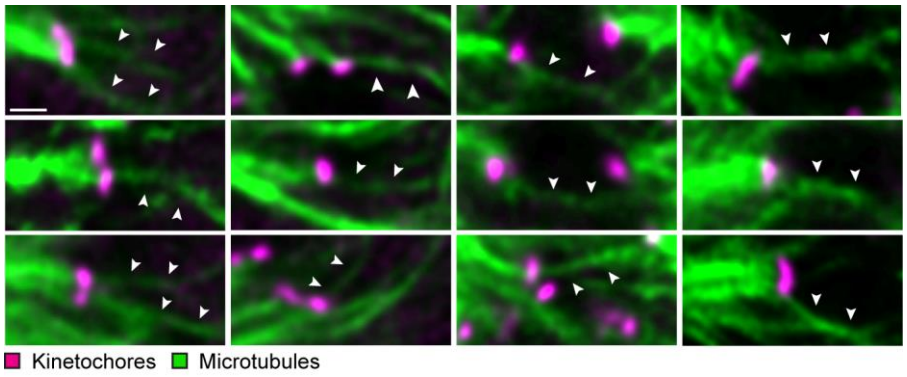

Fig. S8. Examples of merotelic kinetochore-microtubule attachments in oocytes fixed close to anaphase onset.

Twelve additional examples of merotelic kinetochore-microtubule attachments in cold-treated human oocytes fixed close to anaphase onset and immunostained for kinetochores (CREST; magenta) and microtubules (α-tubulin; green). Arrowheads denote merotelically attached microtubules. All images were deconvolved. Scale bar, 1 μm.

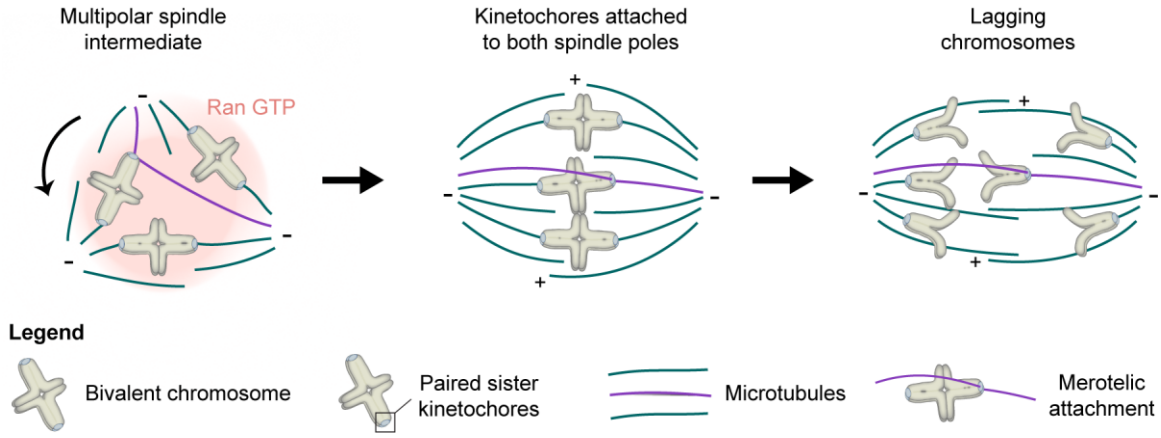

Fig. S9. Scheme illustrating how errors during chromosome-mediated spindle assembly could lead to chromosome segregation defects in human oocytes.

During meiosis I, the homologous chromosomes are associated with each other to form a bivalent chromosome, in which the two sister kinetochores function as a single kinetochore. In human oocytes, microtubules are first nucleated on chromosomes instead of MTOCs in a Ran-GTP-dependent manner. The kinetochores become randomly attached to microtubules in the early stages of spindle assembly. These initially random attachments then need to be sorted into a functional bipolar spindle. Our data suggest that human oocytes are inefficient in correcting kinetochore-microtubule attachments, and that error-correction is incomplete when human oocytes progress into anaphase. Progression into anaphase with these abnormal kinetochore-microtubule attachments (highlighted in purple) can lead to lagging chromosomes, which put the oocyte at risk of aneuploidy due to inappropriate partitioning of chromosomes between the egg and the polar body upon ingression of the cytokinetic furrow. Our data show that the frequency of lagging chromosomes correlates with the degree of spindle instability. One possible explanation for this correlation is that spindle instability and multipolar spindle intermediates hinder the establishment of accurate kinetochore-microtubule attachments. Another possible explanation is that spindle instability is a consequence of the chromosomes' inability to form correct bipolar attachments, which could for instance be due to defects in chromosome or kinetochore morphology.

Movie S1. Meiosis in live human oocyte.

Live human oocyte expressing H2B-mRFP1 (chromosomes) and EGFP-MAP4 (microtubules). *z* projection of four sections, every 5 µm. The magenta/green spheres in the cytoplasm correspond to autofluorescent lipofuscin bodies frequently present in human oocytes (*35*). Scale bar, 10 µm. Time is displayed in hours; NEBD at 2 hours. An additional example is shown in Fig. 1A.

Movie S2. 3D volume reconstructions of MI and MII spindles in human oocytes.

3D volume reconstructions of metaphase I (left) and metaphase II (right) spindles in fixed human oocytes stained for microtubules (α-tubulin). 3D volume reconstructions were generated in Imaris from *z* stacks of sixty one sections, every 0.3 µm. See also fig. S2, A and C. Scale bar, 5 µm.

Movie S3. Microtubules are first nucleated on chromosomes in human oocytes.

z stack of high resolution images of kinetochores (CREST, magenta), microtubules (α-tubulin, green) only (right), and together with chromosomes (Hoechst, cyan) (left) in human oocyte fixed during early microtubule nucleation (~4 hours after NEBD). All channels were deconvolved. Scale bar, 3 µm. See also fig. S4.

Movie S4. Spindle assembly in human oocytes is Ran-GTP-dependent.

Live human oocytes expressing H2B-mRFP1 (chromosomes) and EGFP-MAP4 (microtubules) upon microinjection with Ran T24N (right) or BSA (left). *z* projection of four or six sections, every 3 or 5 µm. The magenta/green spheres in the cytoplasm correspond to autofluorescent lipofuscin bodies frequently found in human oocytes (*35*). Scale bar, 10 µm. Time displayed in hours. An additional example is shown in Fig. 2D.

Movie S5. Spindle instability in human oocyte.

Live human oocyte expressing EGFP-MAP4 (microtubules). *z* projection of five sections, every 3 µm. Scale bar, 10 µm. Time is displayed in hours. See also Fig. 3A.

Movie S6. 3D volume reconstructions of kinetochore-microtubule attachments in human oocytes.

3D volume reconstructions of kinetochores (CREST, magenta), chromosomes (Hoechst, cyan) and microtubules (α-tubulin, green) in cold-treated human oocytes fixed during early (left) or late (right) spindle assembly. 3D volume reconstructions were generated in Imaris from *z* stacks of fifty seven sections, every 0.3 µm. All channels were deconvolved. Background signal outside of the spindle area was masked in kinetochore channel (magenta). Scale bar, 3 µm. See also Fig. 4, A and B.

References and Notes

1. S. I. Nagaoka, T. J. Hassold, P. A. Hunt, Human aneuploidy: Mechanisms and new insights into an age-old problem. *Nat. Rev. Genet.* **13**, 493–504 (2012). Medline doi:10.1038/nrg3245

2. K. A. Knouse, J. Wu, C. A. Whittaker, A. Amon, Single cell sequencing reveals low levels of aneuploidy across mammalian tissues. *Proc. Natl. Acad. Sci. U.S.A.* **111**, 13409–13414 (2014). Medline doi:10.1073/pnas.1415287111

3. F. Pacchierotti, I. D. Adler, U. Eichenlaub-Ritter, J. B. Mailhes, Gender effects on the incidence of aneuploidy in mammalian germ cells. *Environ. Res.* **104**, 46–69 (2007). Medline doi:10.1016/j.envres.2006.12.001

4. C. Templado, F. Vidal, A. Estop, Aneuploidy in human spermatozoa. *Cytogenet. Genome Res.* **133**, 91–99 (2011). Medline doi:10.1159/000323795

5. A. Danylevska, K. Kovacovicova, T. Awadova, M. Anger, The frequency of precocious segregation of sister chromatids in mouse female meiosis I is affected by genetic background. *Chromosome Res.* **22**, 365–373 (2014). Medline doi:10.1007/s10577-014-9428-6

6. Materials and methods are available as supplementary materials on *Science* Online.

7. C. A. Gemzell, Induction of ovulation with human pituitary gonadotrophins. *Fertil. Steril.* **13**, 153–168 (1962). Medline

8. M. Held, M. H. Schmitz, B. Fischer, T. Walter, B. Neumann, M. H. Olma, M. Peter, J. Ellenberg, D. W. Gerlich, CellCognition: Time-resolved phenotype annotation in high-throughput live cell imaging. *Nat. Methods* **7**, 747–754 (2010). Medline doi:10.1038/nmeth.1486

9. M. Schuh, J. Ellenberg, Self-organization of MTOCs replaces centrosome function during acentrosomal spindle assembly in live mouse oocytes. *Cell* **130**, 484–498 (2007). Medline doi:10.1016/j.cell.2007.06.025

10. Z. Holubcová, G. Howard, M. Schuh, Vesicles modulate an actin network for asymmetric spindle positioning. *Nat. Cell Biol.* **15**, 937–947 (2013). Medline doi:10.1038/ncb2802

11. A. Kolano, S. Brunet, A. D. Silk, D. W. Cleveland, M. H. Verlhac, Error-prone mammalian female meiosis from silencing the spindle assembly checkpoint without normal interkinetochore tension. *Proc. Natl. Acad. Sci. U.S.A.* **109**, E1858–E1867 (2012). Medline doi:10.1073/pnas.1204686109

12. G. Manandhar, H. Schatten, P. Sutovsky, Centrosome reduction during gametogenesis and its significance. *Biol. Reprod.* **72**, 2–13 (2005). Medline doi:10.1095/biolreprod.104.031245

13. D. Szöllösi, J. Mandelbaum, M. Plachot, J. Salat-Baroux, J. Cohen, Ultrastructure of the human preovulatory oocyte. *J. In Vitro Fert. Embryo Transfer* **3**, 232–242 (1986). Medline doi:10.1007/BF01132810

14. A. H. Sathananthan, K. Selvaraj, M. L. Girijashankar, V. Ganesh, P. Selvaraj, A. O. Trounson, From oogonia to mature oocytes: Inactivation of the maternal centrosome in humans. *Microsc. Res. Tech.* **69**, 396–407 (2006). Medline doi:10.1002/jemt.20299

15. A. H. Sathananthan, Ultrastructure of human gametes, fertilization and embryos in assisted reproduction: A personal survey. *Micron* **44**, 1–20 (2013). Medline doi:10.1016/j.micron.2012.05.002

16. S. J. Pickering, M. H. Johnson, P. R. Braude, E. Houliston, Cytoskeletal organization in fresh, aged and spontaneously activated human oocytes. *Hum. Reprod.* **3**, 978–989 (1988). Medline

17. D. E. Battaglia, P. Goodwin, N. A. Klein, M. R. Soules, Influence of maternal age on meiotic spindle assembly in oocytes from naturally cycling women. *Hum. Reprod.* **11**, 2217–2222 (1996). Medline doi:10.1093/oxfordjournals.humrep.a019080

18. D. E. Battaglia, N. A. Klein, M. R. Soules, Changes in centrosomal domains during meiotic maturation in the human oocyte. *Mol. Hum. Reprod.* **2**, 845–851 (1996). Medline doi:10.1093/molehr/2.11.845

19. M. A. George, S. J. Pickering, P. R. Braude, M. H. Johnson, The distribution of α- and γ-tubulin in fresh and aged human and mouse oocytes exposed to cryoprotectant. *Mol. Hum. Reprod.* **2**, 445–456 (1996). Medline doi:10.1093/molehr/2.6.445

20. R. Heald, R. Tournebize, T. Blank, R. Sandaltzopoulos, P. Becker, A. Hyman, E. Karsenti, Self-organization of microtubules into bipolar spindles around artificial chromosomes in *Xenopus* egg extracts. *Nature* **382**, 420–425 (1996). Medline doi:10.1038/382420a0

21. R. E. Carazo-Salas, G. Guarguaglini, O. J. Gruss, A. Segref, E. Karsenti, I. W. Mattaj, Generation of GTP-bound Ran by RCC1 is required for chromatin-induced mitotic spindle formation. *Nature* **400**, 178–181 (1999). Medline doi:10.1038/22133

22. O. J. Gruss, R. E. Carazo-Salas, C. A. Schatz, G. Guarguaglini, J. Kast, M. Wilm, N. Le Bot, I. Vernos, E. Karsenti, I. W. Mattaj, Ran induces spindle assembly by reversing the inhibitory effect of importin α on TPX2 activity. *Cell* **104**, 83–93 (2001). Medline doi:10.1016/S0092-8674(01)00193-3

23. E. Karsenti, I. Vernos, The mitotic spindle: A self-made machine. *Science* **294**, 543–547 (2001). Medline doi:10.1126/science.1063488

24. R. E. Carazo-Salas, O. J. Gruss, I. W. Mattaj, E. Karsenti, Ran-GTP coordinates regulation of microtubule nucleation and dynamics during mitotic-spindle assembly. *Nat. Cell Biol.* **3**, 228–234 (2001). Medline doi:10.1038/35060009

25. C. Klebe, F. R. Bischoff, H. Ponstingl, A. Wittinghofer, Interaction of the nuclear GTP-binding protein Ran with its regulatory proteins RCC1 and RanGAP1. *Biochemistry* **34**, 639–647 (1995). Medline doi:10.1021/bi00002a031

26. J. Dumont, S. Petri, F. Pellegrin, M. E. Terret, M. T. Bohnsack, P. Rassinier, V. Georget, P. Kalab, O. J. Gruss, M. H. Verlhac, A centriole- and RanGTP-independent spindle assembly pathway in meiosis I of vertebrate oocytes. *J. Cell Biol.* **176**, 295–305 (2007). Medline doi:10.1083/jcb.200605199

27. J. Cesario, K. S. McKim, RanGTP is required for meiotic spindle organization and the initiation of embryonic development in *Drosophila*. *J. Cell Sci.* **124**, 3797–3810 (2011). Medline doi:10.1242/jcs.084855

28. D. Cimini, B. Moree, J. C. Canman, E. D. Salmon, Merotelic kinetochore orientation occurs frequently during early mitosis in mammalian tissue cells and error correction is achieved by two different mechanisms. *J. Cell Sci.* **116**, 4213–4225 (2003). Medline doi:10.1242/jcs.00716

29. T. S. Kitajima, M. Ohsugi, J. Ellenberg, Complete kinetochore tracking reveals error-prone homologous chromosome biorientation in mammalian oocytes. *Cell* **146**, 568–581 (2011). Medline doi:10.1016/j.cell.2011.07.031

30. A. Obradors, M. Rius, G. Daina, L. Ramos, J. Benet, J. Navarro, Whole-chromosome aneuploidy analysis in human oocytes: Focus on comparative genomic hybridization. *Cytogenet. Genome Res.* **133**, 119–126 (2011). Medline doi:10.1159/000324233

31. M. Faddy, R. Gosden, K. Ahuja, K. Elder, Egg sharing for assisted conception: A window on oocyte quality. *Reprod. Biomed. Online* **22**, 88–93 (2011). Medline doi:10.1016/j.rbmo.2010.08.009

32. L. Rienzi, F. Martinez, F. Ubaldi, M. G. Minasi, M. Iacobelli, J. Tesarik, E. Greco, Polscope analysis of meiotic spindle changes in living metaphase II human oocytes during the freezing and thawing procedures. *Hum. Reprod.* **19**, 655–659 (2004). Medline doi:10.1093/humrep/deh101

33. L. A. Jaffe, M. Terasaki, Quantitative microinjection of oocytes, eggs, and embryos. *Methods Cell Biol.* **74**, 219–242 (2004). Medline doi:10.1016/S0091-679X(04)74010-8

34. L. Strickland, G. von Dassow, J. Ellenberg, V. Foe, P. Lenart, D. Burgess, Light microscopy of echinoderm embryos. *Methods Cell Biol.* **74**, 371–409 (2004). Medline doi:10.1016/S0091-679X(04)74016-9

35. J. Otsuki, Y. Nagai, K. Chiba, Lipofuscin bodies in human oocytes as an indicator of oocyte quality. *J. Assist. Reprod. Genet.* **24**, 263–270 (2007). Medline doi:10.1007/s10815-007-9130-0